Minimum doping densities for pn-junctions

Thomas Kirchartz[1,2*], David Cahen[3]

[1]IEK5-Photovoltaik, Forschungszentrum Jülich, 52425 Jülich, Germany
[2]Fac. of Engineering and CENIDE, Univ. of Duisburg-Essen, Carl-Benz-Str. 199, 47057 Duisburg, Germany
[3]Department of Materials and Interfaces, Weizmann Institute of Science, Rehovoth 76100, Israel

* author for correspondence, email: t.kirchartz@fz-juelich.de

In their article, Cui et al.[1] describe the fabrication and characterization of planar *pn*-junction solar cells based on lead-halide perovskites. The formation of a *pn*-junction is noteworthy given the doping densities, measured using the Hall effect, which were reported to vary from N_D = 1×10^{12} cm^{-3} to 8×10^{12} cm^{-3} for the solution-processed *n*-type layer and to equal $N_A = 8\times10^{9}$ cm^{-3} for the evaporated *p*-type layer. While these devices outperform their counterparts that are supposedly un-doped, the results raise three important questions: are the reported doping densities high enough to change the electrostatic potential distribution in the device from that for the un-doped ones; are the doping densities high enough for the *pn*-junction to remain intact under typical photovoltaic operation conditions; and is a *pn*-junction beneficial for photovoltaic performance given the typical properties of lead-halide perovskites.

The first two questions can be answered by considering semiconductor device physics. The first criterion that the doping densities of the two layers of a *pn*-junction have to satisfy is to ensure that the depletion width $w = \sqrt{2\varepsilon_0\varepsilon_r V_{bi}/qN_{A/D}}$ caused by the doping is substantially smaller than the total absorber layer thickness *d*. Thus, the doping densities have to fulfill $N_{A/D} > 2\varepsilon_0\varepsilon_r V_{bi}/qd^2$ (*q*: electron charge; ε_0: permittivity of vacuum; ε_r: relative permittivity; V_{bi}: built-in voltage). This yields a minimum doping concentration of ~10^{16} cm^{-3} given the reported thickness $d \approx 500$ nm and typical values for the relative permittivity $\varepsilon_r \approx 30$ [2] and for the built-in voltage $V_{bi} \approx 1$ V. Although we do not know the exact V_{bi} value for the present or other perovskite solar cell geometries, it cannot be much smaller than the cell's voltage at the maximum power point in order to avoid S-shaped *I-V* curves[3] and, therefore, has to be around 1 V or higher. Even using 8×10^{12} cm^{-3}, the highest doping density reported by Cui et al., we obtain depletion widths of ~20 µm (Supplementary Figure 1) which is much wider than the thickness of halide perovskite thin film in these solar cells. We also note that such depletion width is wider than in other (non-Si) thin-film solar cells.

This lower limit of ~10^{16} cm^{-3} for the doping concentration applies at thermal equilibrium, e.g. 0 V in the dark. At typical operating conditions of a solar cell, photogenerated charge carriers are created and if their concentrations, *n* and *p*, exceed the doping concentrations, the *pn*-

junction will disappear. At the maximum power point, the product *np* of electron and hole densities is $np \geq n_i^2 \exp\left(qV_{mpp}/kT\right)$, where n_i is the intrinsic carrier concentration, V_{mpp} is the voltage at the maximum power point and kT/q is the thermal voltage. The ≥ sign is necessary because the quasi-Fermi level splitting inside the device is always slightly higher than the externally measured voltage due to finite quasi-Fermi level gradients, needed to drive current.[4] For the doping densities to be still effective at V_{mpp}, the product $N_D N_A$ has to exceed *np* at the maximum power point. The V_{mpp} reported by Cui et al. is 0.89 V leading to $np \approx 6.1 \times 10^{24}$ cm^{-6} which is about two orders of magnitude higher than the highest $N_D N_A$ value, using the reported doping densities, $\approx 6.4 \times 10^{22}$ cm^{-6}. Thus, also in this way we find that the measured doping densities are much lower than needed to exceed the *np* value, deduced from the experimental data, while 10^{16} cm^{-3} donor and acceptor densities would have been able to satisfy both criteria.

To sum up our observations, Figure 1 shows the band diagrams under one sun illumination at $V = 0.89$ V, simulated with the software SCAPS,[5,6] for the doping densities reported by Cui et al. (Figure 1a), 10^{16} cm^{-3} (Figure 1b), and 10^{17} cm^{-3} (Figure 1c).

The band diagram in Figure 1**a** corresponds exactly to the one without doping (see Supplementary Figs. 2 and 3). Due to the band alignment assumed in the simulation, there is an excess of electrons leading to a convex shape of the conduction and valence band edges. In Figure 1**b** and **c** the doping becomes apparent with the conduction band edge being visibly closer to the electron quasi-Fermi level in the entire *n*-type region (blue shaded) than in the *p*-type region (red shaded region).

Another way of verifying that the obtained doping densities are insufficient to achieve a functional *pn*-junction at relevant photovoltaic operating conditions is to compare the difference in Fermi levels determined by Cui et al. using X-ray photoemission spectroscopy and shown in Fig. 3b in ref. [1] for films that are made to be similar to the *n*- and *p*-type regions. The maximum difference in Fermi levels shown is 0.73 eV, which is fairly consistent with the observed doping densities, but is again substantially less than $qV_{mpp} = 0.89$ eV.

While the process used by Cui et al. to obtain the purported *pn*-junction undeniably leads to higher efficiencies, we have proven that – considering the reported doping densities - it is not the doping that causes this improvement. In addition, we note that the drift-diffusion simulation shown in Fig. 2c in ref. [1] is performed using doping densities > 10^{17} cm^{-3} (as reported by Cui et al. Supplementary Table 4 in ref. [1]); indeed, such densities would suffice to create a real *pn* junction (cf. Fig. 1**c** and Supplementary Figure 4), but they are orders of magnitude higher than the experimentally measured values reported by Cui et al.

Our third question above – if a pn-junction in lead-halide perovskite solar cells is a target worth pursuing – is more challenging. This question has no generic answer, because the ideal band diagram for a solar cell depends heavily on the material properties. If the diffusion length is long enough and charge collection is efficient as is the case in high efficiency lead-halide perovskite solar cells, the key question for maximizing the voltage per extracted carrier is how high the recombination rate is for a given defect density and capture cross section and how high the ideality factor is. The first two would reduce the open-circuit voltage, while ideality factors > 1 would reduce the fill factor.[7,8] Both losses are maximized for the scenario where $n\sigma_n=p\sigma_p$ holds in a large part of the absorber volume,[9] where σ_n and σ_p are the capture cross sections for electrons and holes into the defect that dominates recombination. In order to avoid the condition $n\sigma_n=p\sigma_p$, doping may be helpful as shown in Fig. 2, because it induces an asymmetry at least in n vs. p that may help to reduce the absorber volume where $n\sigma_n=p\sigma_p$ to a small region.[10] Thus, *pn*-junctions in lead-halide perovskites could indeed be helpful to achieve higher efficiencies if deep defect densities and carrier mobilities will not be adversely affected by higher doping densities and if those higher doping densities can actually be achieved technologically.

This last point may well be key as a *pn*-junction is not a thermodynamically stable situation; rather it is a kinetically stabilized one.[11] The relatively high diffusion coefficients for atomic/ionic species in the Pb halide perovskites that have been reported in the literature, will decrease such stabilization. More importantly, for a defect to persist within a material, any defect formation energy has to be less than the reaction free energy for decomposition of the material,[12] a condition that limits bulk doping densities beyond those dictated by thermodynamics. In practice, in lead-halide perovskite films the measured doping densities are determined by their external and internal surfaces and interfaces, making the defect chemistry and physics of those key to possible practical *pn*-junctions with such films.

In light of these considerations, while ref. 1 reports an effective way of doping perovskites, which resulted in device efficiency improvement, we have shown that no functional pn-junction can be present in the described devices; thus, other factors must lead to the reported improved device efficiencies.

Methods

The simulations were performed using the software SCAPS (http://scaps.elis.ugent.be). The current-voltage characteristics of solar cells were simulated under a standard AM1.5G spectrum with 100 mW/cm^2 intensity across a 0-1.3 V voltage range. The parameters used in the simulation are reported in Table 1. Thickness, band gap and electron affinity, mobility and doping

densities of the Spiro-OMeTAD and TiOx contact layers are chosen to be identical to those in ref. [1]. Relative permittivity of 30 was chosen based on the findings of ref. [2]. As for the effective density of state (DOS), the values in ref. [1] appeared too high. As effective masses are typically reported to be in the range of 0.1 to 0.3, we chose effective densities of states of 2×10^{18} cm^{-3}.[13] This reduction in effective DOS makes lower doping densities more important so it is better suited to give lower limits of relevant doping concentrations. The radiative recombination coefficient, not corrected for photon recycling, is set as to obtain a radiative open-circuit voltage of ~1.32V for perovskites with band gaps of ~1.6 eV.[14] Surface recombination was neglected as considered less relevant given that there are basically no minority carriers that could lead to charge recombination in the transport layers. The dominant source of recombination used to adjust the V_{oc} to the experimental values in ref. [1] was the Shockley–Read–Hall (SRH) lifetime in the perovskite itself. We found that a lifetime of 20 ns for electrons and holes fits the experimental data well.

For simplicity, the optical model was a simple Lambert-Beer like absorption with an absorption coefficient given by $\alpha = A\sqrt{E - E_g}$, where A is a prefactor with the unit $cm^{-1}eV^{-1/2}$, E is the energy and E_g is the band gap. The work function of the left and right contact were set to 4 eV for the front contact (cathode) and 5.1 eV for the back contact (anode) leading to good Fermi level alignment with the Fermi level in the ETL and HTL.

Table 1: Parameters used for the simulations.

Parameter	**TiO_x**	**Perovskite (n-type)**	**Perovskite (p-type)**	**Spiro-OMeTAD**
thickness (nm)	20	480	60	200
relative permittivity	100	30	30	3
band gap (eV)	3.2	1.6	1.6	2.91
electron affinity (eV)	4	3.93	3.93	2.2
effective DOS CB (cm^{-3})	10^{21}	2×10^{18}	2×10^{18}	10^{18}
effective DOS VB (cm^{-3})	2×10^{20}	2×10^{18}	2×10^{18}	10^{18}
SRH lifetime $\tau_n = \tau_p$ (ns)	-	20	20	-
radiative recombination coefficient (cm^3/s)	0	3×10^{11}	3×10^{11}	0
electron mobility (cm^2/Vs)	6×10^{-3}	10	10	10^{-3}
hole mobility (cm^2/Vs)	6×10^{-3}	10	10	10^{-3}
absorption constant ($cm^{-1}eV^{-0.5}$)	0	7×10^4	7×10^4	0
doping density (cm^{-3})	5×10^{19}	variable	variable	10^{18} (p-type)

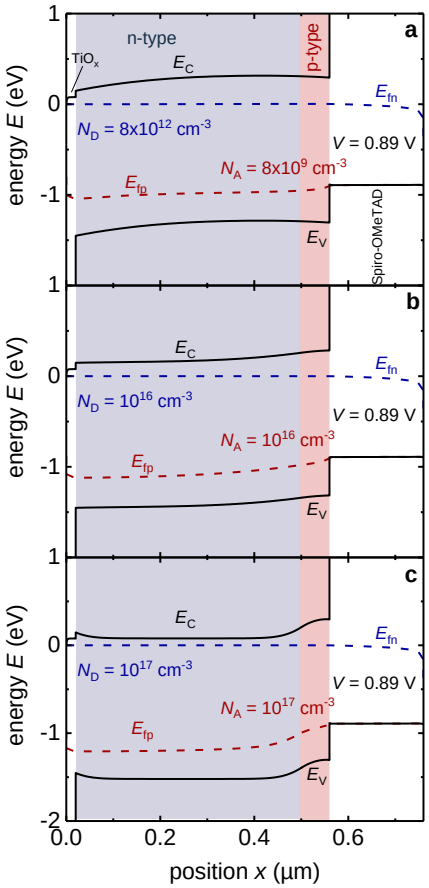

Fig. 1 | Effect of doping on the band diagram of halide perovskite solar cells. Band diagram of a TiO_x (20 nm)/n-type perovskite (blue shade) (480 nm)/p-type perovskite (red shade) (60 nm)/Spiro-OMeTAD (200 nm) stack with the doping density being **a** as given in ref. [1], **b** 10^{16} cm^{-3} for both donor and acceptor concentration and **c** 10^{17} cm^{-3} for both donor and acceptor concentration. The quasi-Fermi levels of electrons (E_{fn}) and holes (E_{fp}) are depicted with dashed lines. All other simulation parameters are found in the Methods section. The simulations are done under 1 sun illumination and at a forward bias of V = 0.89V which corresponds to the maximum power point of the certified cell presented by Cui et al. [1].

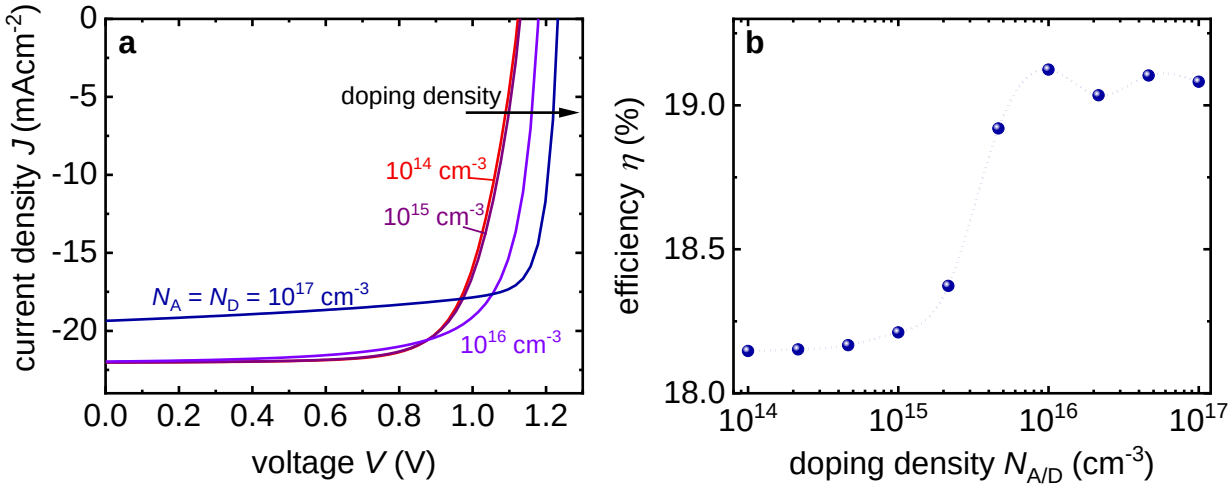

Fig. 2 | Effect of doping on the photovoltaic parameters of perovskite solar cells. a Current-voltage curves, simulated using the same parameters used for Fig. 1 but with the doping densities varied from 10^{14} to 10^{17} cm^{-3}. Donor and acceptor concentration are assumed identical. The results show that up to around 10^{15} cm^{-3}, no effect is visible. For higher doping densities J_{sc} decreases and V_{oc} goes up due to a reduction of the volume in which $n\sigma_n = p\sigma_p$. Note that the simulation assumes that in the perovskite, recombination is via a deep trap that has equal capture cross sections for electrons and holes ($\sigma_n = \sigma_p$). **b** Efficiency as a function of doping density (in logarithmic scale) showing a peak at a doping density of 10^{16} cm^{-3} that holds for the parameters used here. The dotted line is a guide to the eye. The results show that even if the Hall measurements, which are problematic on samples with very low carrier densities and modest mobilities, lead to an underestimation of doping densities in ref.[1] by a few orders of magnitude, our conclusion stands.

Competing interest

The authors declare no competing financial interests.

Author contributions

TK performed the simulations, all quantitative comparisons and wrote most of the manuscript. DC initiated the work and wrote the last part of the manuscript.

Bibliography

1 Cui, P. *et al.* Planar p-n homojunction perovskite solar cells with efficiency exceeding 21.3%. *Nature Energy* **4**, 150-159 (2019).

2 Sendner, M. *et al.* Optical phonons in methylammonium lead halide perovskites and implications for charge transport. *Materials Horizons* **3**, 613-620, doi:10.1039/C6MH00275G (2016).

3 Tress, W., Leo, K. & Riede, M. Influence of Hole-Transport Layers and Donor Materials on Open-Circuit Voltage and Shape of I-V Curves of Organic Solar Cells. *Advanced Functional Materials* **21**, 2140-2149 (2011).
4 Würfel, U., Cuevas, A. & Würfel, P. in *IEEE Journal of Photovoltaics* Vol. 5 461-469 (2015).
5 Burgelman, M., Verschraegen, J., Degrave, S. & Nollet, P. Modeling thin-film PV devices. *Progress in Photovoltaics* **12**, 143-153 (2004).
6 Burgelman, M., Nollet, P. & Degrave, S. Modelling polycrystalline semiconductor solar cells. *Thin Solid Films* **361**, 527-532 (2000).
7 Green, M. A. Solar cell fill factors: General graph and empirical expressions. *Solid-State Electronics* **24**, 788-789 (1981).
8 Stocks, M. J., Cuevas, A. & Blakers, A. W. in *Progress in Photovoltaics: Research and Applications* Vol. 4 35-54 (John Wiley & Sons, Ltd, 1996).
9 Green, M. A. in *Progress in Photovoltaics: Research and Applications* Vol. 4 375-380 (John Wiley & Sons, Ltd, 1996).
10 Kirchartz, T., Bisquert, J., Mora-Sero, I. & Garcia-Belmonte, G. Classification of solar cells according to mechanisms of charge separation and charge collection. *Physical Chemistry Chemical Physics* **17**, 4007-4014, doi:10.1039/C4CP05174B (2015).
11 Guillemoles, J. F., Lubomirsky, I., Riess, I. & Cahen, D. in *The Journal of Physical Chemistry* Vol. 99 14486-14493 (American Chemical Society, 1995).
12 Rakita, Y., Lubomirsky, I. & Cahen, D. When defects become 'dynamic': halide perovskites: a new window on materials? *Materials Horizons* **6**, 1297-1305, doi:10.1039/C9MH00606K (2019).
13 Staub, F. *et al.* Beyond Bulk Lifetimes: Insights into Lead Halide Perovskite Films from Time-Resolved Photoluminescence. *Physical Review Applied* **6**, 044017 (2016).
14 Tvingstedt, K. *et al.* Radiative efficiency of lead iodide based perovskite solar cells. *Sci. Rep* **4**, 6071 (2014).